Surg Radiol Anat (2018) 40:159–164
DOI 10.1007/s00276-017-1935-7

ORIGINAL ARTICLE

Visualization of the cavum septi pellucidi, cavum Vergae, and cavum veli interpositi using magnetic resonance imaging

Satoshi Tsutsumi[1] · Hisato Ishii[1] · Hideo Ono[2] · Yukimasa Yasumoto[1]

Received: 21 August 2017 / Accepted: 20 October 2017 / Published online: 1 November 2017

Abstract
Purpose The morphology of the cavum septi pellucidi (CSP), cavum Vergae (CV), and cavum veli interpositi (CVI) has been infrequently explored with neuroimaging. The aim of the present study was to delineate these cavities using magnetic resonance (MR) imaging.
Methods A total of 71 patients were enrolled in the present study. Following initial examinations with conventional MR sequences, constructive interference in steady-state (CISS) sequence was performed in the coronal and sagittal sections for 60 and 11 patients, respectively.
Results The coronal CISS images at the level of the aqueduct showed two distinct morphologies of the CV roof, one formed by the fornices with varying degrees of conjugation and the other formed by the corpus callosum with completely separated fornices. Appearance of the CSP was classified into four distinct types. Furthermore, the CVI presented two distinct appearances.
Conclusions Typically, the CSP, CV, and CVI present with asymptomatic conditions with morphological variabilities. Visualization of the CSP, CV, and CVI using the CISS sequences may be useful when managing lesions affecting these cavities.

Keywords Cavum septi pellucidi · Cavum Vergae · Cavum veli interpositi · Morphological variability · CISS sequence

✉ Satoshi Tsutsumi
shotaro@juntendo-urayasu.jp

[1] Department of Neurological Surgery, Juntendo University Urayasu Hospital, 2-1-1 Tomioka, Urayasu, Chiba 279-0021, Japan

[2] Division of Radiological Technology, Medical Satellite Yaesu Clinic, Tokyo, Japan

Introduction

The cavum Vergae (CV) and cavum veli interpositi (CVI) are acknowledged as developmental anatomical variants located in the midline of the brain, while the cavum septi pellucidi (CSP) are consistently found in fetal life and newborns. Clinicopathological implications of these cavities have not been determined yet. Embryologically, the CSP and CV are assumed to be devoid of cerebrospinal fluid (CSF) and any ependymal lining. In contrast, the CVI is considered to be a true cerebral cistern communicating with the quadrigeminal cistern backward [5, 13, 17, 19]. Previous study suggested that the CSP and CV might resorb the CSF due to the pressure gradient produced under unique circumstances, for instance, when they were communicating with the lateral ventricle [14]. Occurrences of these cavities and their clinicopathological implications have been investigated previously, primarily in the pediatric populations with magnetic resonance imaging (MRI), computed tomography scans, and pneumoencephalography [1–3, 6, 8, 10, 11, 13, 15]. However, in those studies, diagnostic criteria of the cavities were not clearly mentioned; therefore, inconsistent outcomes were observed. The CVI that involves vascular and membranous structures has been explored in cadaveric specimens [12, 16, 19]. The CSP, CV, and CVI can be the structures to be managed when approaching lesions located in and around the third ventricle through the transcallosal–transchoroidal and transcallosal–transforniceal–transchoroidal approaches [7, 18]. To our knowledge, morphologies of these cavities are yet to be documented. So in the present study, our aim was to delineate the CSP, CV, and CVI using MR imaging.

Materials and methods

The present retrospective study included a total of 71 patients who visited our hospital on an outpatient basis, during two periods, one from January 2010–April 2011 and the other from June 2012–August 2012. The patients presented with headache, dizziness, tinnitus, hearing disturbance, hemisensory disturbance, and seizure. The patient cohort during first visit consisted of 60 patients, including 30 men and 30 women, with a mean age of 49.5 years (age range: 9–77 years). Among those 60 patients, three were male pediatric patients younger than 13 years. All of them were developmentally normal. The patient cohort during the second visit consisted of 11 adult patients, including seven men and four women, with a mean age of 43.7 years (age range: 20–70 years). Initial neurological examination and interviews confirmed that none of the 71 patients had a history of previous intracranial hemorrhage, cerebral infarction, meningitis, ventriculitis, neurodegenerative disease, traumatic brain injury, intracerebral and intraventricular cysts, hydrocephalus, brain tumor, or psychotic disorders. These conditions were excluded during initial examination with axial T1- and T2-weighted images (WIs), T2-gradient

Table 1 Incidences of the cavum septi pellucidi (CSP), cavum Vergae (CV), and cavum veli interpositi (CVI)

	Coronal CISS $N=60$	Sagittal CISS $N=11$
CSP	25 (42%)	6 (55%)
CV	4 (7%)	1 (9%)
CVI	30 (50%)	6 (55%)

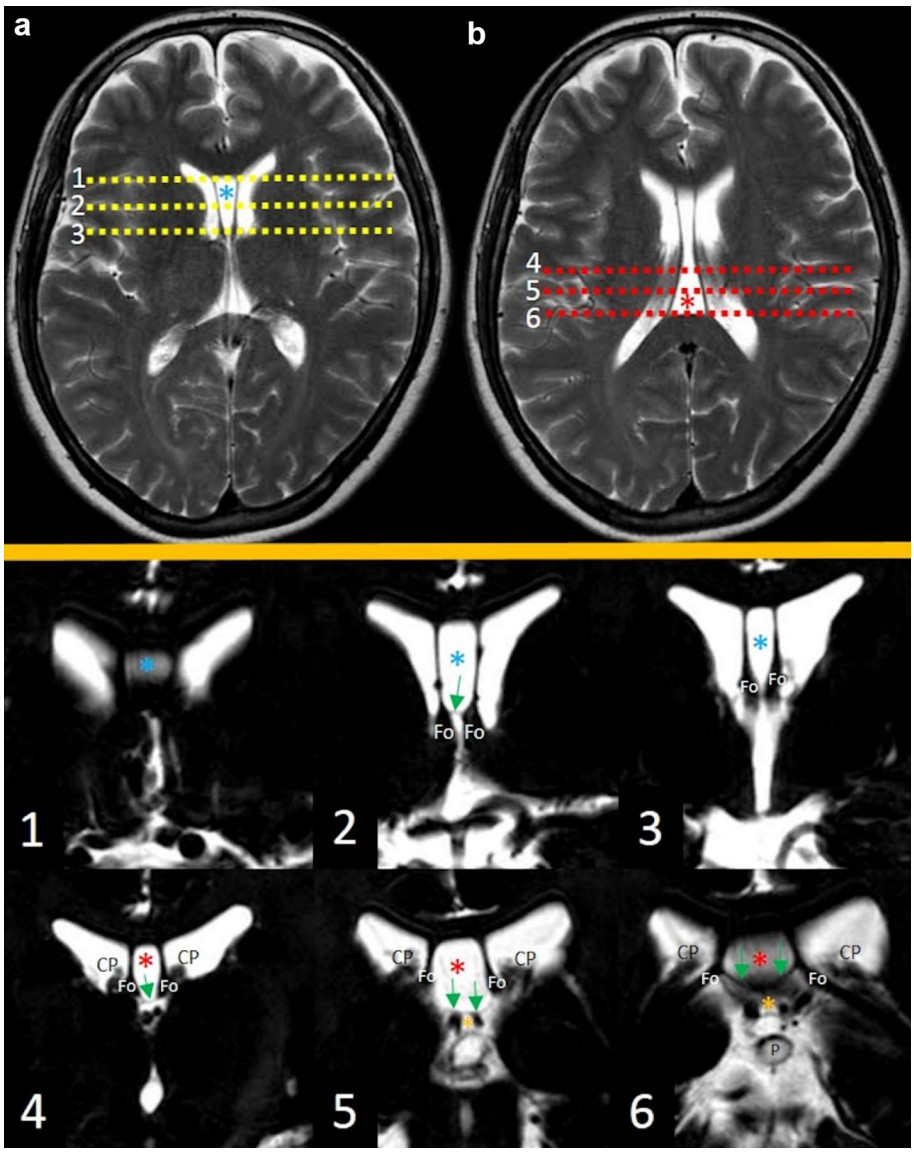

Fig. 1 Axial T2-weighted magnetic resonance images at the level of the foramen of Monro (**a**) and that at the lowest level of the body of the lateral ventricles (**b**), and coronal constructive interference steady-state images at the six corresponding levels in **a** and **b** of a patient (1–6: lower column) showing the cavum septum pellucidum, cavum Vergae, cavum veli interpositum, and their relevant structures. *CP* choroid plexus, *Fo* body of the fornix, *P* pineal gland, blue asterisk: cavum septi pellucidi; orange asterisk: cavum veli interpositi; red asterisk: cavum Vergae; green arrows: floors of the cavum septi pellucidi and cavum Vergae. (Color figure online)

echo, fluid-attenuated inversion recovery, and diffusion-weighted sequences. The T2WIs at the level of the foramen of Monro and that at the lowest level of the body of the lateral ventricles were used as references for identifying the CSP, CV, and CVI. The parameters for obtaining the T2WIs were as follows: repetition time (TR) of 4266 ms, echo time (TE) of 95 ms, slice thickness of 5.00 mm, interslice gap of 0.5 mm, matrix of 400 × 269 dimension, field view of 230 mm × 230 mm × 216 mm dimension, flip angle of 90°, and a scan duration of 1 min 59 s. The patients then underwent imaging with thin-sliced, constructive interference steady-state (CISS) sequences in coronal and sagittal sections. Both examinations involved the entire lateral and third ventricles. Coronal CISS images were obtained from all patients who presented during the first visit, while sagittal images were obtained from all patients who presented during the second visit. The parameters for obtaining the coronal images were as follows: TR of 2000 ms, TE of 311 ms, slice thickness of 2.00 mm, interslice gap of 0 mm, matrix of 320 × 274 dimension, field view of 160 mm × 160 mm × 100 mm dimension, flip angle of 90°, and scan duration of 5 min 30 s. The parameters for the sagittal images were as follows: TR of 1960 ms, TE of 289 ms, slice thickness of 0.60 mm, interslice gap of 0 mm, matrix of 160 × 160 dimension, field view of 160 mm × 160 mm × 132 mm dimension, flip angle of 90°, and a scan duration of 4 min 30 s.

All imaging sequences were performed using a 3.0 T MR scanner (Achieva R2.6; Philips Medical Systems, Best, The Netherlands). Imaging data were transferred to a workstation (Virtual Place Lexus64. 64 edition; AZE, Tokyo, Japan) and independently analyzed by two authors (S.T. and H.I.). The shape and extent of the CSP, CV, and CVI were assessed on the serial coronal and sagittal CISS images. The present study was performed in accordance with our institution's guidelines for human research. Written informed consents were obtained from all patients.

Results

The CSP, CV, and CVI were identified in 40 (67%) out of the 60 patients who underwent coronal CISS sequences. A total of 25 patients (42%) presented with CSP, four patients (7%) presented with the CV, and 30 patients (50%) presented with CVI. Among three pediatric patients, one was identified with CSP, while the other was identified with CVI. In the remaining one patient, no CSP, CV, or CVI was detected. These cavities were detected in ten of the 11 (91%) adult patients who underwent sagittal CISS sequence, comprising of six patients (55%) presented with CSP, one patient (9%) presented with CV, and six patients (55%) presented with CVI (Table 1).

The CSP, CV, and CVI were assessed both on the coronal and sagittal CISS images with axial T2WIs at the level of the foramen of Monro and at the lowest level of the body of the lateral ventricles used as references. These cavities were delineated as well-circumscribed, fluid-filled spaces divided by the medial walls of the lateral ventricles, fornices, corpus callosum, and the roof as well as the floor of the CVI (Figs. 1, 2, 3). The coronal CISS images at the level of the aqueduct showed two distinct morphologies of CV roof. In one type, the roof was formed by the fornices with varying degrees of conjugation and found in 73% of the 30 identified patients. In the other type, the roof was formed by corpus callosum for

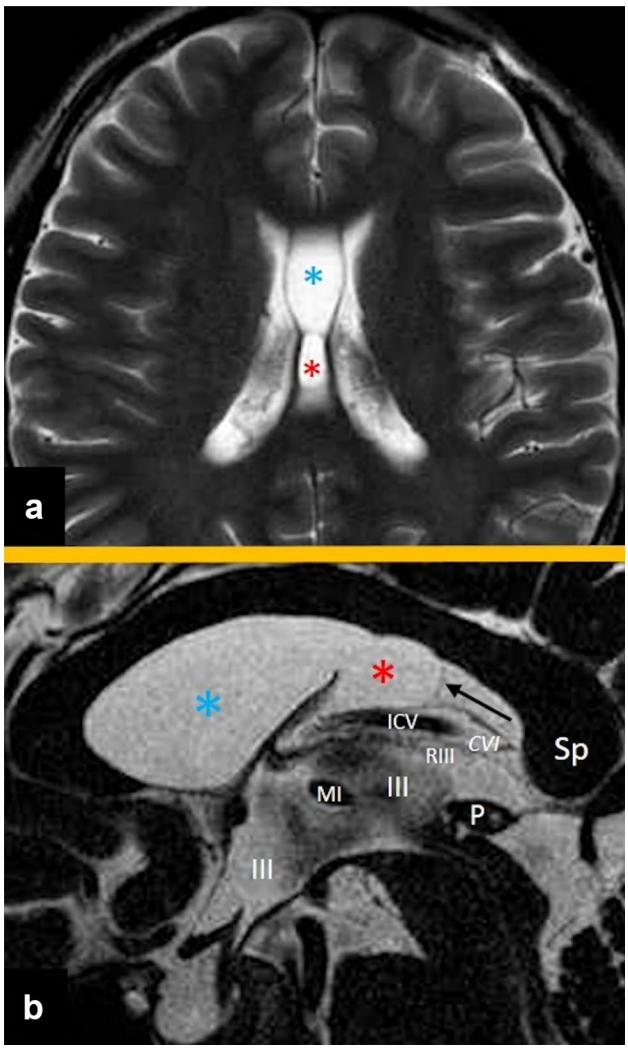

Fig. 2 Axial T2-weighted magnetic resonance images at the lowest level of the body of the lateral ventricles (**a**) and midsagittal constructive interference steady-state image (**b**) in a patient showing the cavum septum pellucidum and cavum Vergae. *CVI* cavum veli interpositi, *ICV* internal cerebral vein, *MI* massa intermedia, *RIII* roof of the third ventricle, *Sp* splenium of the corpus callosum, *III* third ventricle. Blue asterisk: cavum septi pellucidi; red asterisk: cavum Vergae; arrow: membranous structure found in the cavum Vergae. (Color figure online)

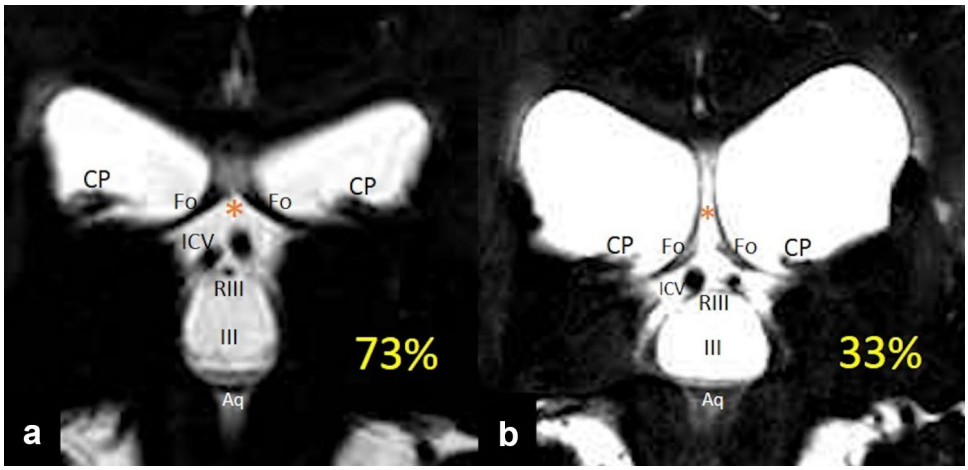

Fig. 3 Coronal constructive interference steady-state images of different patients performed at the level of the aqueduct showing two types of the roof of the cavum veli interpositi. **a** The roof is formed by the fornices forming varying degrees of conjugation, found in 73% of the 30 identified patients. **b** The roof is formed by the corpus callosum for completely separate two fornices, found in 33% of the patients. *Aq* aqueduct, *CP* choroid plexus. Orange asterisk: cavum veli interpositi. (Color figure online)

completely separated bilateral fornices and detected in 33% of the patients (Fig. 3). The shapes of the CSP were classified into four distinct types based on the morphological characteristics. The Type I CSP presented with a slit-like appearance and found in 32% of the 25 identified patients. The Type II CSP presented with an oval-shaped appearance and found in 48% of the patients. The Type III CSP presented with a round appearance and found in 16% of the patients. The Type IV CSP presented with an irregular-shaped appearance and identified in 4% of the patients (Fig. 4). Furthermore, the CVI presented two distinct types of appearances: (a) a small CVI with short superior-to-inferior dimensions found in 20% of the ten identified patients and (b) a large CVI with long superior-to-inferior dimensions found in 80% of the patients (Fig. 5). In summary, the coronal CISS sequences were useful in evaluating superior-to-inferior and lateral dimensions of the CSP and CV, while sagittal CISS sequences were useful in delineating the anterior-to-posterior and superior-to-inferior dimensions of the CVI.

Discussion

The CISS sequence is a gradient-echo MR imaging technique used to delineate a wide range of pathologies that proves to be useful when routine MR imaging sequences do not provide optimal anatomical information. The increased sensitivity of the CISS sequence is obtained by accentuation of the T2 values between the CSF and targeted structures [4, 9].

In the present study, the CSP, CV, and CVI were identified in 67% of the patients using coronal CISS sequence and 91% of the patients with sagittal CISS sequence. Occurrences of CSP, CV, and CVI were considerably higher than those found in previous studies that provided inconsistent and variable outcomes [1, 2, 8, 10, 13]. Most of the differences probably stemmed from the differences in study design for identifying these cavities, modalities used for

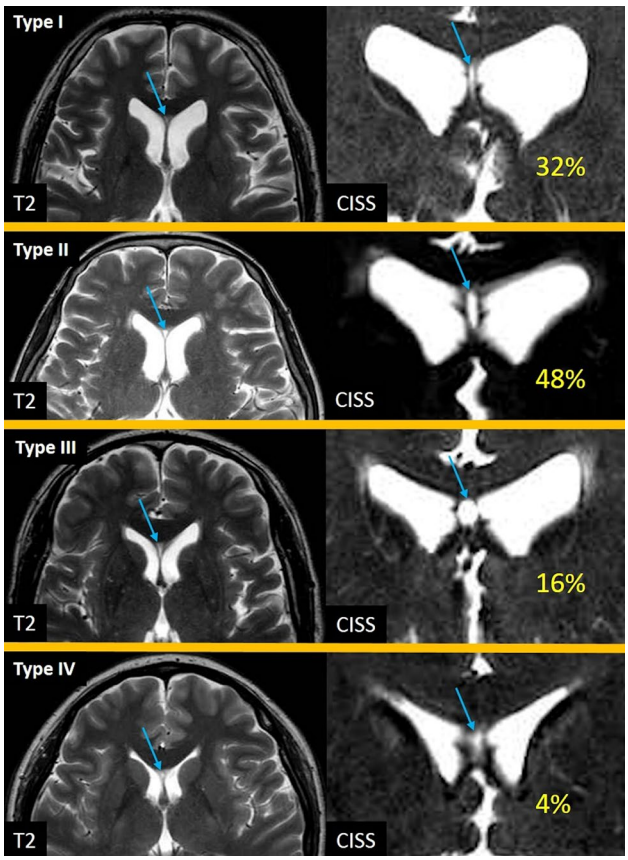

Fig. 4 Axial T2-weighted magnetic resonance images at the level of the foramen of Monro (Types I–IV: left pictures) and coronal constructive interference steady-state images at the midlevel of the cavum septi pellucidi (Types I–IV: right pictures) of different patients showing four distinct morphologies of cavum septi pellucidi and their distribution. Type I: slit type, found in 32% of the 25 identified patients; Type II: oval type, found in 48% of the identified patients; Type III: round type, found in 16% of the identified patients; Type IV: irregular type, found in 4% of the identified patients. Blue arrow: cavum septi pellucidi. (Color figure online)

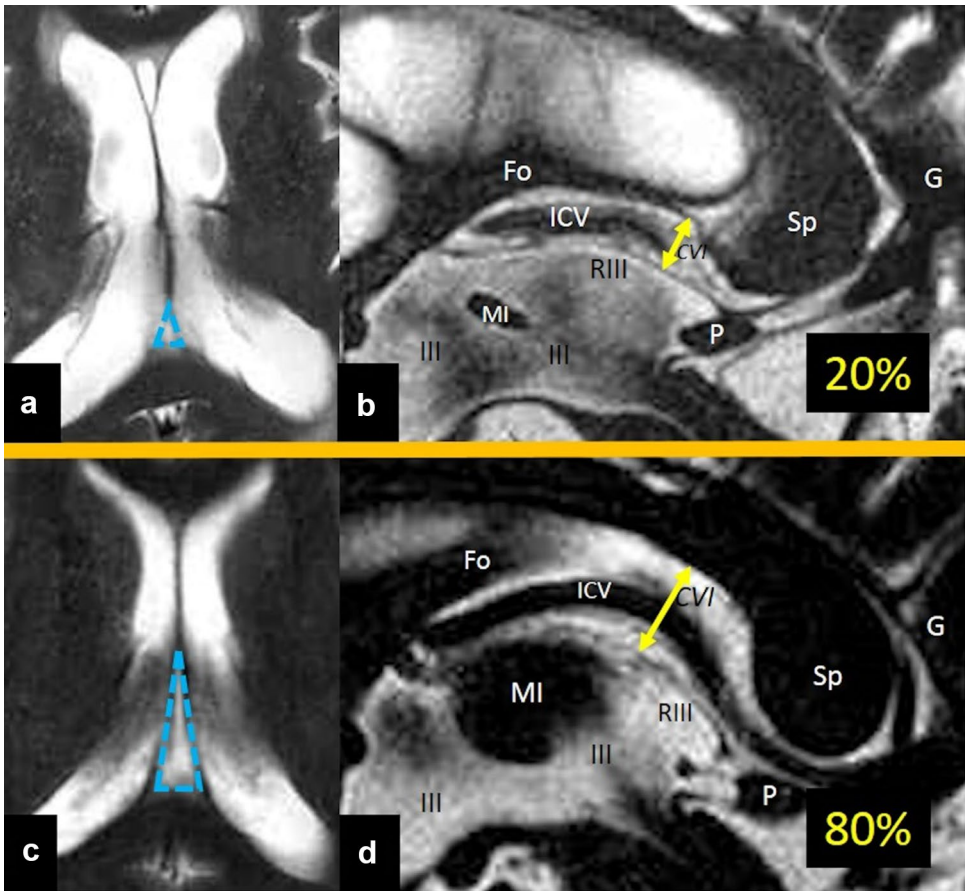

Fig. 5 Axial T2-weighted magnetic resonance images at the lowest level of the body of the lateral ventricles (**a**, **c**) and midsagittal constructive interference steady-state images of the corresponding patients (**b**, **d**) showing different types of the cavum veli interpositum (CVI). Upper column: a small CVI (**a**: triangular area formed by blue dotted lines) with a short superior-to-inferior dimension (**b**: double-headed yellow arrow), found in 20% of the ten identified patients. Lower column: a large CVI (**c**: triangular area formed by blue dotted lines) with a long superior-to-inferior dimension (**d**: double-headed yellow arrow), found in 80%. *G* vein of Galen. (Color figure online)

delineating the cavities, and diagnostic criteria. Given the high prevalence of CSP and CVI, they may present typically asymptomatic conditions as normal variants.

The coronal CISS images at the level of the aqueduct showed two distinct types. In addition, the shapes of the CSP were classified into four distinct types. Furthermore, morphology of the CVI showed two distinct types. These morphological variabilities may partly explain the inconsistent, highly variable incidences of the CSP and CVI as found in previous studies [1–3, 8, 13, 15]. In the present study, the coronal CISS sequence was assumed to be useful in evaluating the superior-to-inferior and lateral dimensions of the CSP and CV, while the sagittal CISS sequence was proved to be advantageous in evaluating the anterior-to-posterior and superior-to-inferior dimensions of the CVI. This may especially be useful when entering into the third ventricle through the transcallosal–transchoroidal and transcallosal–transforniceal–transchoroidal routes in patients with a large CSP, CV, and CVI.

There are several limitations in our study. It was a retrospective investigation lacking random assignment of participants. The two cohorts of participants included different number of individuals, with non-homogeneous age and sex compositions. Furthermore, the CSP, CV, and CVI were assessed only in cohorts without apparent pathologies in and around the areas surrounding them. Despite these limitations, the findings obtained from our study may help to determine appropriate surgical maneuvers while managing lesions affecting such cavities.

Conclusions

Typically, the CSP, CV, and CVI present with asymptomatic conditions and morphological variabilities. Visualization of these structures using the CISS sequence may be useful in managing lesions affecting these cavities.

Acknowledgements This work was not supported by any grant.

Author contributions ST and HO designed this study and performed magnetic resonance imaging. HI and YY analyzed the imaging data. ST wrote the manuscript.

Compliance with ethical standards

Conflict of interest The authors have no conflicts of interest concerning the materials or methods used in the present study or the findings presented in the manuscript.

References

1. Aldur MM, Gürcan F, Başar R, Akşit MD (1999) Frequency of septum pellucidum anomalies in non-psychotic population: a magnetic resonance imaging study. Surg Radiol Anat 21:119–123
2. Aldur MM, Celik HH, Gürcan F, Sancak T (2001) Frequency of cavum veli interpositi in non-psychotic population: a magnetic resonance imaging study. J Neuroradiol 28:92–96
3. Bodensteiner JB, Schaefer GB, Craft JM (1998) Cavum septi pellucidi and cavum Vergae in normal and developmentally delayed populations. J Child Neurol 13:120–121
4. Burmeister HP, Möslein C, Bitter T, Fröber R, Herrmann H, Baltzer PA, Gudziol H, Diezel M, Guntinas-Lichius O, Kaiser WA (2011) In vivo comparison of water displacement method and 3 T MRI for MR-volumetry of the olfactory bulb. Which sequence is appropriate? Acad Radiol 18:1233–1240
5. Ciołkowski MK (2011) Cavum velum interpositum, cavum septum pellucidum and cavum Vergae: a review. Childs Nerv Syst 27:2027–2028
6. Giussani C, Fiori L, Trezza A, Riva M, Sganzerla EP (2011) Cavum veli interpositi: just an anatomical variant or a potentially symptomatic CSF compartmentalization? Pediatr Neurosurg 47:364–368
7. Graziano F, Ganau M, Meccio F, Iacopino DG, Ulm AJ (2015) The transcallosal anterior interforniceal approach: a microsurgical anatomy study. J Neurol Surg B Skull Base 76:183–188
8. Gur RE, Kaltman D, Melhem ER, Ruparel K, Prabhakaran K, Riley M, Yodh E, Hakonarson H, Satterthwaite T, Gur RC (2013) Incidental findings in youths volunteering for brain MRI research. AJNR Am J Neuroradiol 34:2021–2025
9. Held P, Fellner C, Fellner F, Seitz J, Graf S, Hilbert M, Strutz J (1997) MRI of inner ear and facial nerve pathology using 3D MR-RAGE and 3D CISS sequences. Br J Radiol 70:558–564
10. Nakano S, Hojo H, Kataoka K, Yamasaki S (1981) Abe related incidence of cavum septi pellucidi and cavum Vergae on CT scans of pediatric patients. J Comput Assist Tomogr 5:348–349
11. Picard L, Leymarie F, Roland J, Sigiel M, Masson JP, André JM, Renard M (1976) Cavum veli interpositi. Roentgen anatomy–pathology and physiology. Neuroradiology 10:215–220
12. Rhoton AL Jr (2002) The lateral and third ventricles. Neurosurgery 51(4 Suppl):S207–S271
13. Saba L, Anzidei M, Raz E, Suri J, Piga M, Grassi R, Catalano C (2013) MR and CT of brain's cava. J Neuroimaging 23:326–335
14. Sencer A, Sencer S, Turantan I, Devecioğlu O (2001) Cerebrospinal fluid dynamics of the cava septi pellucidi and vergae. Case report. J Neurosurg 94:127–129
15. Sundarakumar DK, Farley SA, Smith CM, Maravilla KR, Dighe MK, Nixon JN (2015) Absent cavum septum pellucidum: a review with emphasis on associated commissural abnormalities. Pediatr Radiol 45:950–964
16. Tubbs RS, Louis RG Jr, Wartmann CT, Loukas M, Shoja MM, Apaydin N, Oakes WJ (2008) The velum interpositum revisited and redefined. Surg Radiol Anat 30:131–135
17. Tubbs RS, Krishnamurthy S, Verma K, Shoja MM, Loukas M, Mortazavi MM, Cohen-Gadol AA (2011) Cavum velum interpositum, cavum septum pellucidum, and cavum Vergae: a review. Childs Nerv Syst 27:1927–1930
18. Vitorino Araujo JL, Veiga JCE, Wen HT, de Andrade AF, Teixeira MJ, Otoch JP, Rhoton AL Jr, Preul MC, Spetzler RF, Figueiredo EG (2017) Comparative anatomical analysis of the transcallosal-transchoroidal and transcallosal-transforniceal-transchoroidal approaches to the third ventricle. J Neurosurg 127:209–218
19. Zhang XA, Qi S, Fan J, Huang G, Peng J, Xu J (2012) The distribution of arachnoid membrane within the velum interpositum. Acta Neurochir (Wien) 154:1711–1715